Stimuli-Mediated Structural Interchange Between Pd_6 and Pd_{12} Architectures: Selective Recognition of E-Stilbene by the Pd_6 Architecture and its Photoprotection

*Medha Aggarwal, Ranit Banerjee, Neal Hickey, and Partha Sarathi Mukherjee**

Abstract: The dynamic behaviour of metal-ligand bonding cultivates stimuli-mediated structural transformations in self-assembled molecular architectures. The propensity of synthetically designed self-assembled systems to interchange between higher-order architectures is increased multi-fold when the building blocks have higher conformational degrees of freedom. Herein, we report a new ligand, (2,7-bis(di(pyridin-4-yl)amino)-9*H*-fluoren-9-one) (**L**), which, upon self-assembly with a *cis*-[(ethylene-1,2-diamine)Pd(NO_3)$_2$] acceptor (**M**), resulted in the formation of a $\mathbf{M_6L_3}$ trifacial barrel (**C1**) in water. Interestingly, during crystallization, a rare $\mathbf{M_{12}L_6}$ triangular orthobicupola architecture (**C2**) was generated along with **C1**. **C2** could also be generated in solution via the application of several stimuli. **C1** in aqueous media could stabilize one *trans*-stilbene (**tS**) or *cis*-stilbene (**cS**) molecule in its cavity, with a selectivity for the former from their mixture. Moreover, **C1** acted as an effective host to prevent the otherwise facile photoisomerization of **tS** to **cS** inside its hydrophobic cavity under UV irradiation. Conversely, the visible-light-induced reverse isomerization of encapsulated **cS** to encapsulated **tS** could be achieved readily due to the better stabilization of **tS** within the cavity of **C1** and its transparency to visible light. A multi-functional system was therefore designed, which at the same time is stimuli-responsive, shows isomer selectivity, and photoprotects *trans*-stilbene.

Introduction

Coordination-driven self-assembly enables the construction of complex and precisely defined discrete architectures reminiscent of the structural complexity observed in biological systems.[1–6] The main advantage of this strategy is that it involves no synthetic complexities and is generally high-yielding, unlike traditional covalent bond-forming approaches.[7–9] These synthetic systems can exhibit similar substrate-binding capability,[10–12] conformational flexibility,[13,14] and responsiveness to external stimuli such as temperature,[15,16] concentration,[17,18] solvent,[19–20] counter-anion,[21–23] or guest molecules,[24–27] thus making them valuable tools for studying enzyme-like behavior in a controlled setting. There are two essential aspects of designing enzyme-mimicking coordination cages. Firstly, the cavities of the self-assembled host should be such that it can stabilize guest molecules via different non-covalent interactions. In this context, barrel-like molecular architectures with tubular cavities surrounded by continuous walls embedded with desirable functional moieties and open portals (windows) have been found to be compelling.[28] The confinement of guest molecules within the pockets of such hosts has led to the emergence of several applications, including sensing,[29–33] encapsulation of substrates for carrying out organic transformations in aqueous media and stabilization of transition states that facilitates catalysis,[34–42] separation of isomers by selective encapsulation,[43–48] and stabilization of reactive molecules or otherwise unstable intermediates,[49–52] biological applications,[53–55] and light-harvesting.[56–59] Secondly, the propensity to undergo enzyme-like structural modulation from a specific architecture to another architecture of comparable stability in the presence of external signals depends upon the lability of the metal-ligand bond and the conformational flexibility of the building units.[60–62] Generally, for the construction of molecular barrels, symmetric tetra-topic rigid ligands are self-assembled with 90° Pd(II)/Pt(II) acceptors.[28,63] To facilitate such cages with stimuli-responsive behavior, it is imperative to design tetra-dentate ligand with a higher degree of conformational and coordinative flexibility with respect to the ligand coordination vectors.

Stilbene and its derivatives exhibit photochromic behavior, existing as *trans* and *cis*-geometric isomers that interconvert upon exposure to UV andvisible light irradiation, respectively. The ratio of these isomers can fluctuate after multiple photo-irradiation cycles, contingent upon the stability of their respective photo-stationary states.[64] Additionally, both isomers are often produced in varying proportions during synthesis, necessitating selective recognition of one isomer in a mixture.[65]

[*] M. Aggarwal, R. Banerjee, Prof. P. S. Mukherjee
Department of Inorganic and Physical Chemistry
Indian Institute of Science
Bangalore 560012 (India)
E-mail: psm@iisc.ac.in

N. Hickey
Department of Chemical and Pharmaceutical Sciences
University of Trieste
Trieste 34127 (Italy)

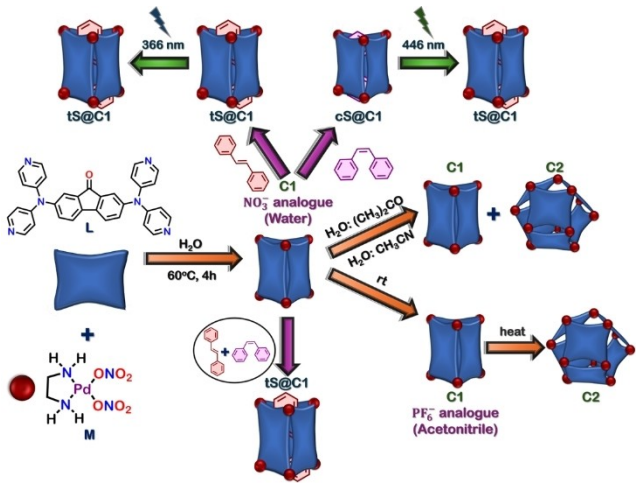

Scheme 1. Schematic representation of the synthesis of trifacial barrel **C1** and its conversion to **C2** on implementation of various external stimuli. **C1** selectively housed one molecule of **tS** from a mixture of **cS** and **tS**. **C1** shielded encapsulated **tS** from photo-isomerizing to **cS** under UV irradiation. Under visible light irradiation **cS@C1** was converted to **tS@C1** due to better stabilization of **tS** within the cavity of **C1**.

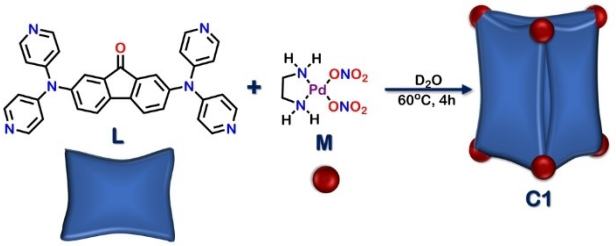

Scheme 2. Schematic representation for the synthesis of **C1**.

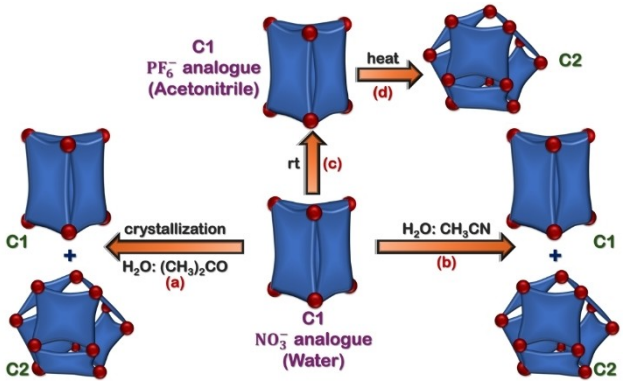

Scheme 3. Schematic representation of stimuli-responsive behaviour of **C1**: (a) during crystallization by diffusion of acetone into aqueous solution of **C1** (NO_3^- analogue), (b) after addition of miscible proportions of acetonitrile to aqueous solution of **C1** (NO_3^- analogue), (c) after counter-anion exchange to PF_6^- analogue at room temperature in acetonitrile, and (d) after heating the solution of PF_6^- analogue in acetonitrile at 55 °C for 12 h.

Herein, we report the synthesis of a new tetra-topic fluorenone-derived flexible ligand **L**. Self-assembly of **L** with *cis*-[(en)Pd(NO_3)$_2$] (**M**) in aqueous media resulted in the formation of a simple and symmetric trifacial barrel (**C1**) (Schemes 1 and 2) [en: ethylene-1,2-diamine]. The dynamic nature of Pd–N bonding afforded interplay between Pd_6 (**C1**) and Pd_{12} (**C2**) architectures in the presence of different stimuli. Crystallization afforded the formation of a rare triangular orthobicupola (**C2**) along with **C1**. Moreover, the addition of acetonitrile to the NO_3^- analogue of **C1** in water efficiently affected the partial transformation of **C1** to **C2**. Next, the counter-anion dependency was investigated by converting the NO_3^- analogue to the PF_6^- analogue. The acetonitrile soluble PF_6^- analogue was found to exist as a mixture of **C1** and **C2** at room temperature, with **C1** as the major product. Interestingly, upon heating the mixture, **C2** was formed and was found stable even at room temperature. The system was thus dependent on crystallization, solvent, and counter anion, which provided a platform for interplay between structurally distinct Pd_6 and Pd_{12} architectures (Schemes 1 and 3). The NO_3^- analogue in aqueous solution existed exclusively as **C1**, which provided an optimum cavity for encapsulating stilbene isomers via H-bonding interactions between the free and inwardly directed carbonyl moieties of the host and the alkene protons of the guest. Although both the *trans* (**tS**) and *cis* (**cS**) isomers could be encapsulated within the cavity of **C1**, the former was stabilized more strongly due to exact cavity size and shape matching, leading to a selectivity for the *trans* isomer [**tS**: *trans* stilbene; **cS**: *cis* stilbene]. The photo-switching of **tS** to **cS** occurs readily under UV irradiation. **C1** effectively blocked the photo-induced transformation of encapsulated **tS** to **cS** in aqueous media by more strongly stabilizing **tS** rather than **cS** and absorbing the incoming UV irradiation. On the other hand, **C1** was transparent to visible light thereby, **cS@C1** readily transformed to **tS@C1** under visible light irradiation (Scheme 1). The better stabilization of less polar **tS** within the hydrophobic cavity of **C1** facilitated the transformation. Thus, herein we report a multi-tasking self-assembled system which, on one hand, is stimuli-responsive and, on the other, selectively recognizes, stabilizes and photo-protects one of the geometrical isomers of stilbene in aqueous media - a capability which is under-explored.

Results and Discussion

Synthesis and Characterization of Trifacial Barrel (C1) and Triangular Orthobicupola (C2)

The tetra-pyridyl ligand **L** was synthesized by a copper-catalyzed Ullmann coupling reaction between 2,7-dibromo-9*H*-fluoren-9-one and 4,4′-dipyridylamine in diphenyl ether following standard procedures for similar substrates.[66] The newly synthesized ligand **L** was completely characterized using NMR and ESI-MS techniques (Figures S4–S6). Next, the self-assembly reaction between **L** and *cis*-[(en)Pd(NO_3)$_2$] acceptor (**M**) was carried out in a 1:2 molar ratio at 60 °C in D_2O for 4 h, which afforded an almost clear orange solution

(Scheme 2). The ^{1}H NMR spectrum displayed five distinct peaks in the aromatic region with significant shifts of the ligand protons without any additional splitting, which indicates the formation of a simple and symmetric molecular barrel (Figure 1a, S7) architecture. ^{1}H-DOSY NMR further confirmed the presence of only one molecular species with a diffusion coefficient, $D = 1.69\times10^{-10}$ m^2/s and hydrodynamic radius, r = 14.4 Å (Figures 1b, S8).

To obtain single crystals suitable for X-ray diffraction, acetone vapors were slowly diffused into the in situ reaction mixture in H_2O. Interestingly, two different types of crystals were obtained (**C1** and **C2**). The single-crystal structure analysis of **C1** unambiguously confirmed the formation of a simple and symmetric molecular barrel of composition $\mathbf{M_6L_3}$. **C1** crystallizes in hexagonal space group *P6$_3$/m* wherein the three ligands (**L**) assume vertical orientations and are clipped to six Pd(II) acceptors (**M**) at the vertices, forming a tube-like architecture (Figure 2). In **C1**, all three ligands experience the same time-averaged chemical environment, which corroborates well with the symmetric and unsplit ^{1}H NMR in D_2O, indicating **C1** to be the species present in aqueous solution (Figure 1a, S7). Furthermore, the non-solvated radius obtained from the crystal structure (r = 13.3 Å) (calculated by considering the distance of the centroid from the farthest atom) was slightly shorter but very close to the hydro-dynamic radius (r = 14.4 Å) obtained from DOSY (Figure 1b, S8). Although the data is not of the highest quality, the single-crystal structure analysis of **C1** unambiguously confirmed the formation of a simple and symmetric molecular barrel of composition $\mathbf{M_6L_3}$ (see Supporting Information for details).

On the other hand, the single-crystal structure analysis of **C2** confirmed the formation of a metallacage $\mathbf{M_{12}L_6}$ with an unusual triangular orthobicupola architecture resembling Johnson's polyhedron J_{27}. **C2** crystallizes in monoclinic space group *C2/m*. The six tetra-topic ligands (**L**) occupy all the six rectangular faces of the J_{27} polyhedron, while the twelve Pd(II) acceptors (**M**) are present at the vertices, forming a bicupola-like structure with a hexagonal base and open triangular faces (Figure 3). Unlike in **C1**, all the α and β pyridyl protons of ligand (**L**) in **C2** do not experience the same chemical environment and are expected to show multi-fold splitting. Moreover, the non-solvated radius of **C2** (16.6 Å) obtained from the crystal structure is much larger compared to the hydrodynamic radius obtained from ^{1}H DOSY (14.4 Å) (Figure 1b, S8) analysis of the aqueous solution.

These observations confirm that **C1** is the only species present in aqueous solution; however, crystals of both **C1** as well as **C2** were obtained upon slow diffusion of acetone vapor into an aqueous solution of **C1**. These results prompted us to explore whether the diffusing solvent (acetone) or concentration played any role in the generation of **C2** from an aqueous solution of **C1**. Therefore, the ^{1}H NMR spectra were recorded with different fractions of acetone-d_6 added to the D_2O solution of **C1** until precipitation. No significant change apart from slight spectral broadening was observed in ^{1}H NMR spectra, ruling out the role of acetone in modulating the relative amounts of self-assembled architectures **C1** and **C2** in solution (Figure S10). Next, we investigated the concentration dependency in aqueous solution. At lower concentrations (c = 9.6 mM with respect to **L**), only one set of peaks corresponding to **C1** was present. However, as the concentration gradually increased, a new set of peaks started appearing. However, at the saturation limit (where precipitation was observed) (c = 57.8 mM with respect to ligand), only an insignificant

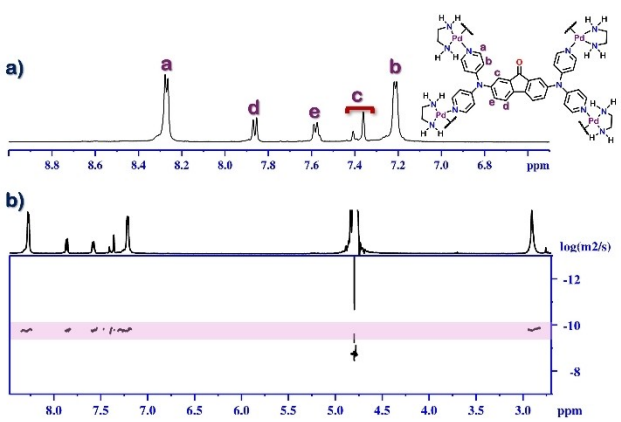

Figure 1. (a) ^{1}H NMR spectrum of cage **C1** and (b) ^{1}H DOSY NMR of **C1** in D_2O at 298 K.

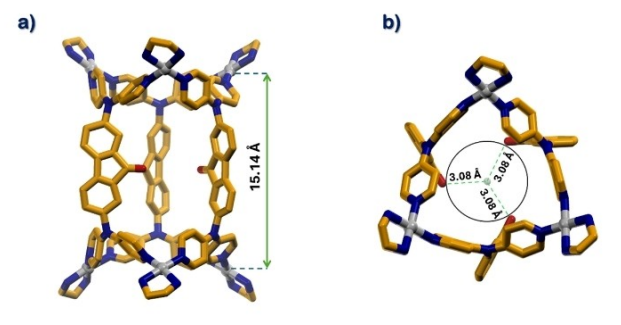

Figure 2. Single crystal structure of **C1**: (a) side view, (b) top view. Colour codes: carbon (yellow), nitrogen (deep blue), oxygen (red) and palladium (grey). Hydrogen atoms, counter-anions, and solvent molecules are omitted for clarity.

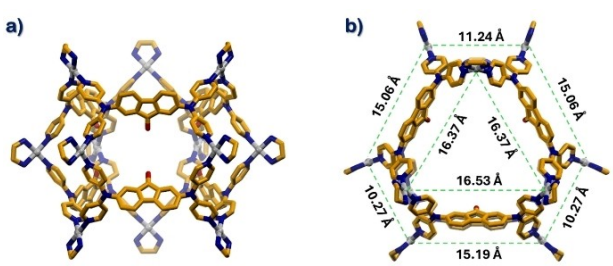

Figure 3. Single crystal structure of **C2**: (a) side view, (b) top view. Colour codes: carbon (yellow), nitrogen (deep blue), oxygen (red) and palladium (grey). Hydrogen atoms, counter-anions, and solvent molecules are omitted for clarity.

amount of the new architecture, probably **C2**, was obtained along with major product **C1** (Figure S11).

Thus, although new small peaks were observed at higher concentrations, the highest concentration (saturation limit) was not enough to generate a characterizable amount of **C2** in solution, which was generated upon crystallization. These experiments confirmed that crystallization (highest degree of concentration) acted as a stimulus to generate a new triangular orthobicupola cage (**C2**) along with a simple trifacial barrel (**C1**) from **C1**, the only component present in aqueous solution.

Solvent, Counter-anion and Temperature Dependent Structural Interchange Between Trifacial Barrel (C1) and Triangular Orthobicupola (C2)

C2 was not observed in purely aqueous media and could be detected only in crystalline form. We further went on to investigate whether we could generate **C2** in solution by the addition of different proportions of other solvents to the aqueous solution of **C1**. After screening with different solvents, we found new sets of peaks appearing in the ^{1}H NMR upon the addition of acetonitrile to an aqueous solution of **C1**, indicating the generation of a new self-assembled architecture (Figure S13, Scheme 3). ^{1}H NMR of the self-assembled product recorded in a 3:2 D_2O-CD_3CN mixture showed two sets of peaks with two different diffusion coefficients as obtained from ^{1}H DOSY NMR (Figures 4, S14–S16). All the peaks were assigned with the help of 2D ^{1}H-^{1}H COSY NMR (Figure S17). **C1** was found to be the major product with simple and unsplit NMR, whereas the new set of peaks (appearing due to the addition of acetonitrile) showed a four-fold splitting of α and β pyridyl protons of ligands (**L**), indicating the formation of triangular orthobicupola, **C2** (Figure 4, S14 and S15). In a triangular orthobicupola geometry, the pyridyl donors are in two different chemical environments, resulting in different chemical shifts. Moreover, the inward and outward orientations of pyridyl groups, as seen in the single-crystal structure of **C2**, result in a four-fold splitting of α-pyridyl protons (Figures 4a and S15). Further, the diffusion coefficient (D) corresponding to **C2** ($D = 1.55\times10^{-10}$ m^2/s) was much lower compared to the diffusion coefficient (D) for **C1** ($D = 1.99\times10^{-10}$ m^2/s), which is consistent with the larger solvodynamic radius for the triangular orthobicupola (**C2**) (Figure S16). The relative amounts of **C1** and **C2** were found to be 89:11 in the 3:2 D_2O-CD_3CN mixture, as determined from ^{1}H NMR integrations.

To further validate the composition of the assemblies, the NO_3^- analogue of **C1** was converted to its PF_6^- analogue for better ionization and was subjected to ESI-MS analyses in acetonitrile. The ESI-MS analyses confirmed the presence of an assembly with composition $\mathbf{M_6L_3}$ (**C1**). The peaks and isotopic patterns obtained at *m/z* values 1286.3697 (calc.1286.3601), 928.5410 (calc. 928.5290), 713.8301 (calc. 713.8304), and 688.8456 (calc. 688.8452) correspond to $[\mathbf{C1}.9PF_6]^{3+}$, $[\mathbf{C1}.8PF_6]^{4+}$, $[\mathbf{C1}.7PF_6]^{5+}$, and $[\mathbf{C1}.2NO_3.5PF_6.CH_3CN]^{5+}$, respectively (Figures 5a, S22 and S23). However, no isotopic patterns corresponding to an $\mathbf{M_{12}L_6}$ composition (**C2**) were detected in the ESI-MS (Figures S22 and S26). Next, we investigated the temperature dependency by heating the acetonitrile solution of PF_6^- analogue at 55 °C for 12 h. Interestingly, peaks and isotopic patterns corresponding to an $\mathbf{M_{12}L_6}$ (**C2**) composition were detected in ESI-MS with no traces of **C1**. Peaks were obtained at *m/z* = 2002.0162 (calc. 2002.0223), 1572.6139 (calc. 1572.6250), 1286.3477 (calc. 1286.3014), 1081.8786 (calc. 1081.8852), 928.5203 (calc. 928.5290) corresponding to $[\mathbf{C2}.20PF_6]^{4+}$, $[\mathbf{C2}.19PF_6]^{5+}$, $[\mathbf{C2}.18PF_6]^{6+}$, $[\mathbf{C2}.17PF_6]^{7+}$ and $[\mathbf{C2}.16PF_6]^{8+}$ respectively, and the isotopic patterns were also in good agreement with theoretically calculated isotopic patterns (Figures 5b, S24 and S25).

The ^{1}H NMR spectrum further corroborated with the ESI-MS results. The ^{1}H NMR of the PF_6^- analogue in

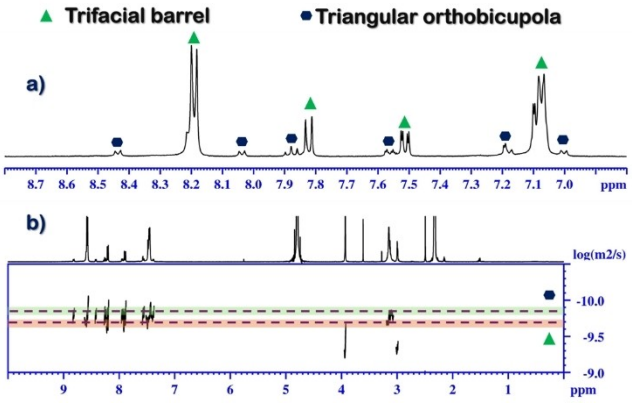

Figure 4. (a) ^{1}H NMR spectrum and (b) ^{1}H DOSY NMR spectrum of a mixture of cages (**C1** and **C2**) in 3:2 D_2O: CD_3CN at 298 K.

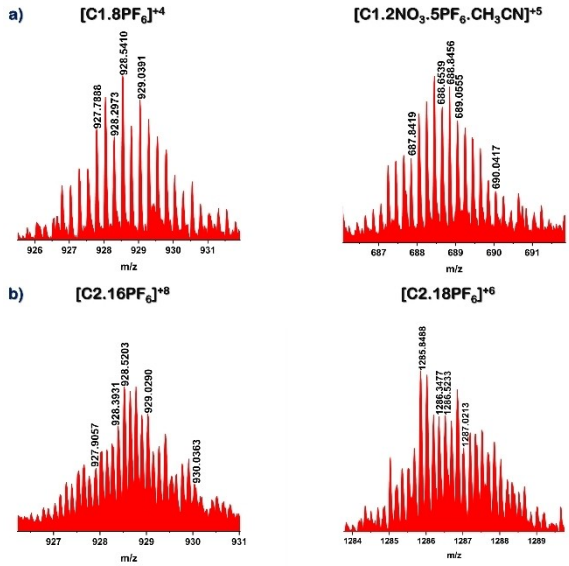

Figure 5. Experimental isotopic patterns of **C1** and **C2** fragments obtained in ESI-MS: (a) $[\mathbf{C1}.8PF_6]^{4+}$ and $[\mathbf{C1}.2NO_3.5PF_6.CH_3CN]^{5+}$ fragments, and (b) $[\mathbf{C2}.16PF_6]^{8+}$ and $[\mathbf{C2}.18PF_6]^{6+}$ fragments.

CD_3CN (Figure S18a) showed mainly one set of peaks (major product) with small peaks corresponding to traces of other self-assembled products at 25 °C (only **C1** could be detected from ESI-MS). The ^{1}H DOSY NMR was recorded, which confirmed the presence of one self-assembled product (major product) with a higher diffusion coefficient ($D = 3.31\times10^{-10}$ m^2/s) corresponding to the trifacial barrel (**C1**) and the other self-assembled architecture (minor product) with a lower diffusion coefficient ($D = 2.51\times10^{-10}$ m^2/s), probably corresponding to triangular orthobicupola (**C2**) (Figure S19). Expectedly, upon gradually heating the solution, the set of peaks corresponding to the minor product (**C2**) emerged, along with the disappearance of peaks corresponding to **C1** (Figure S18a–f, Scheme 3). **C2** was found to be stable at room temperature for weeks in CH_3CN, confirming it to be a stable self-assembled architecture of the PF_6^- analogue in acetonitrile. It is important to mention here that the NO_3^- analogue in the aqueous solution showed no temperature dependence, and the NO_3^- analogue of the trifacial barrel, **C1**, was the thermodynamically stable product in aqueous media (Figure S12). The PF_6^- analogue in acetonitrile, however, did not show any concentration dependency (Figure S21). Stimuli-induced generation of such an unusual triangular ortho-bicupola architecture from a completely different non-isomeric self-assembled product (trifacial barrel) in solution has never been reported to the best of our knowledge.

Host-Guest Chemistry and Photoisomerization Within the Cavity of Trifacial Barrel (C1)

In aqueous media, only the trifacial barrel (**C1**) is present. **C1** possesses a long, tubular cavity of length ca. 15.1 Å and an internal diameter of ca. 6.2 Å and is perfectly suited for encapsulating hydrophobic guest molecules of similar dimensions via non-covalent interactions. The (E)-isomer of 1,2-diphenyl ethene (*trans*-stilbene, **tS**) has a length of *ca.* 11.5 Å, and we expected that it would perfectly fit into the tubular cavity and be stabilized via O···H interactions between the oxygen atoms of fluorenone moieties and guest's C–H protons. This prompted us to carry out the guest encapsulation study with **tS**. The host–guest studies were carried out by treating the aqueous solution of **C1** with an excess of **tS**, and the mixture was stirred at room temperature in the dark for 12 h. The mixture was then centrifuged to remove the excess guest (**tS**). Indeed, several new peaks with multiple splitting were observed in the ^{1}H NMR spectrum corresponding to the host due to the loss of symmetry of the host in the presence of the guest. The peaks corresponding to guest (**tS**) were also highly upfield shifted (compared to the free guest), indicating their encapsulation within the cavity of **C1** (Figures 6a, 6b, S27). Further, ^{1}H DOSY gave a single diffusion coefficient for both the host and guest peaks due to the formation of the host–guest complex [**tS@C1**] (Figure S28). ^{1}H-^{1}H COSY and NOESY were recorded to exactly allocate the host and guest peaks (Figures S29 and S30). Correlations were observed between the protons of the host **C1** (protons a, b, and c) and guest

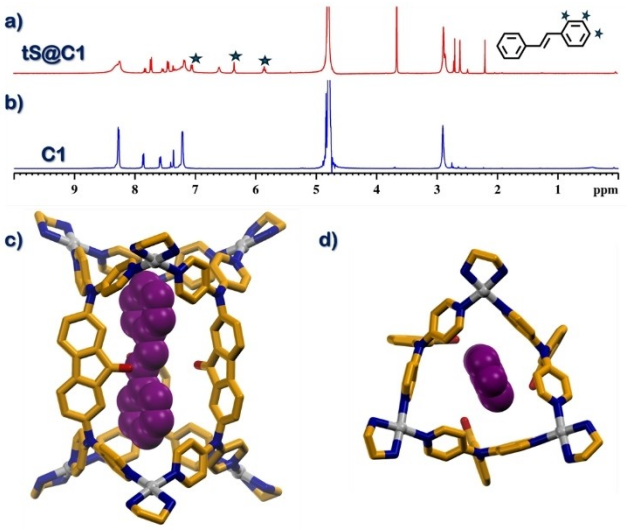

Figure 6. Stacked ^{1}H NMR spectra of (a) host–guest complex **tS@C1** and (b) cage **C1** in D_2O at 298 K. DFT optimized structure of **tS@C1**: (c) side view (d) top view. Colour codes of host: carbon (yellow), nitrogen (deep blue), oxygen (red), palladium (grey). Colour codes of guest: carbon (purple). Hydrogen atoms are omitted for clarity.

(**tS**) in the ^{1}H-^{1}H NOESY NMR due to the proximity of host and guest because of encapsulation of **tS** within the cavity of **C1** [**tS@C1**] (Figure S30). The ^{1}H NMR integration gave the host–guest stoichiometry of 1:1, confirming the encapsulation of one **tS** molecule within the cavity of **C1**. Multiple attempts to obtain crystals for **tS@C1** were unsuccessful. The geometry of the host–guest complex (**tS@C1**) was optimized using the density functional theory (DFT) method by placing one molecule of **tS** within the tubular cavity of **C1**. The **tS** molecule was found to be stabilized via multiple O···H interactions between the fluorenone oxygens directed towards the internal cavity and ethylene C–H and aromatic C–H protons of the encapsulated *trans*-stilbene molecule (Figure 6c, 6d and S42).

Stilbene exists as E and Z geometric isomers. The photo stationary states are stable, but often, mixtures of both forms are present in varying ratios after several photo-irradiation events. Moreover, during the synthesis, both the isomers are generated. Selective recognition of one of the isomers in a mixture is, therefore, a challenging task. The molecular barrel **C1** effectively encapsulates the *trans*-isomer due to the proper size matching of **tS** with the host cavity. Thus, we went on to explore whether **C1** could also house the Z-isomer of stilbene (*cis*-stilbene, **cS**) within its cavity. A D_2O solution of **C1** was treated with one equivalent of **cS**, and the mixture was stirred at room temperature in the dark for 12 h and centrifuged. The ^{1}H NMR of the resulting solution indicated a large upfield shift for the **cS** protons (Figures S32 and S36), indicating the formation of **cS@C1**. Peaks corresponding to the unencapsulated **cS** were also observed due to the slight solubility of **cS** in water (Figures S32 and S36). Competitive host–guest study was next carried out to investigate whether **C1** binds **tS** or **cS** more strongly (Scheme 4). When a 1:1 mixture of

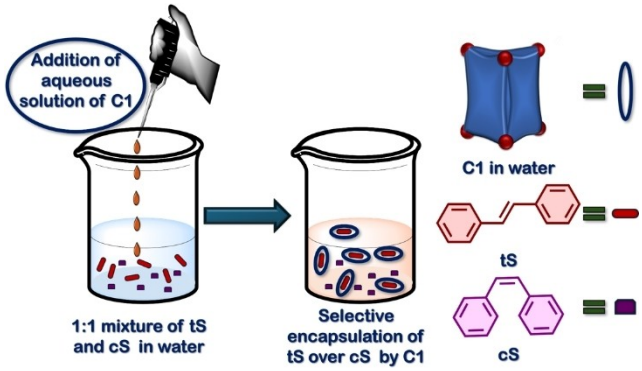

Scheme 4. Schematic representation of selective encapsulation of **tS** over **cS** by **C1**.

cS and **tS** was added to the D_2O solution of **C1**, the ^1H NMR resembled the ^1H NMR of **tS@C1** (Figures 7a, 7b, S34 and S36; Figure 7a: ^1H NMR recorded after **tS + cS** mixture was added to **C1**; Figure 7b: ^1H NMR of **tS@C1**). Free **cS** peaks were also observed (Figures 7a and 7d; Figure 7d: ^1H NMR of **cS**); however, no peaks corresponding to encapsulated **cS** were observed (Figures 7a and 7c; Figure 7c: ^1H NMR recorded after **cS** was added to **C1**, comprising of both free and encapsulated **cS** peaks). This ascertained that the aqueous solution of **C1** was more selective towards the E-isomer (**tS**) than the Z-isomer (**cS**). Further, the structure of **cS@C1** was optimized by the DFT method by placing a **cS** molecule within the cavity of **C1** (Figure 7e, 7f and S43). The single point energy calculations depicted that **tS@C1** was more stable by about 9.5 kcal/mol than **cS@C1**, corroborating with the experimentally observed results (Table S3).

Thus, in aqueous media, **C1** acts as an efficient host for *trans*-stilbene (**tS**) due to the effective size and shape matching of **tS** with the cavity of **C1** and multiple H-bonding interactions between the fluorenone-cores of the host and guest protons. **C1** also weakly stabilizes the *cis* isomer within its cavity. However, from a 1:1 *trans/cis* mixture, it can selectively recognize the *trans* isomer.

Stilbene can be photo-switched from its E-form (**tS**) to Z-form (**cS**) and vice-versa using UV and visible light sources, respectively. The irradiation of free **tS** in chloroform using a light source of 366 nm for 8 h leads to partial photoconversion of **tS** to **cS**, leading to the attainment of a photo-stationary state containing 40 % **cS** and 60 % **tS** (Scheme 5a, Figure S38). Surprisingly, when the host-guest complex, **tS@C1** in aqueous media was irradiated with the same light source for the same time interval, the ^1H NMR of **tS@C1** remained apparently the same and there was no appearance of encapsulated or free **cS** peaks (Figure S39, Scheme 5b). This confirmed that **C1** could act as a shield to prevent the photobleaching of **tS** to **cS** under UV irradiation, which was readily achieved in organic solvents (Scheme 5a and 5b). The photo-shielding ability of **C1** may be attributed to the strong absorption of **C1** in the UV region (Figure S37) leading to UV-light masking, and the higher stability of **tS** compared to **cS** within **C1** and the spatial constraints of **C1**, which hinders free rotation about

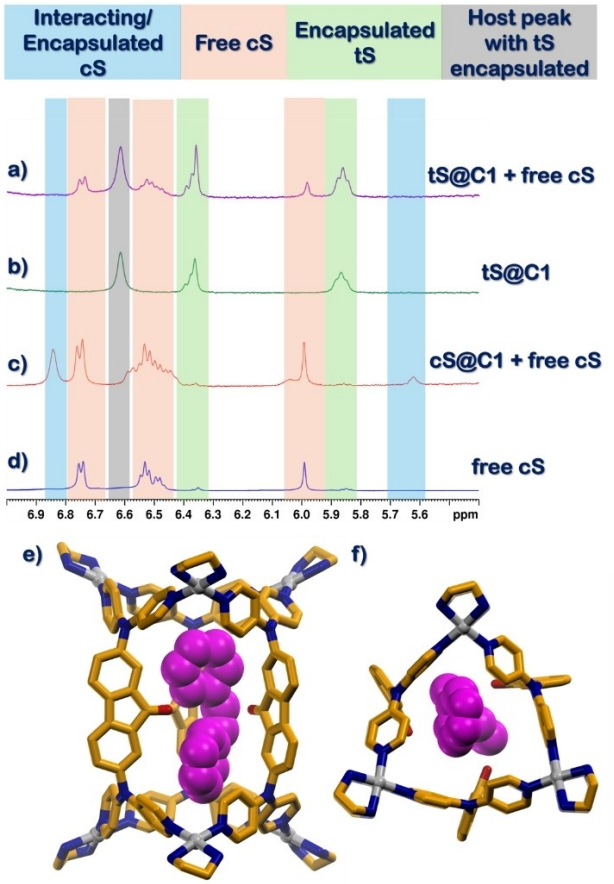

Figure 7. Stacked ^1H NMR spectra (expanded view showing the stilbene protons) of (a) after treatment of **C1** with 1:1 mixture of **tS** and **cS** (**tS@C1** + unencapsulated **cS**), (b) **tS@C1**, (c) after treatment of **C1** with **cS** (both encapsulated **cS** peaks, **cS@C1** and free **cS** are present) (d) free **cS**. The blue band designates interacting/encapsulated **cS** peaks, the light orange band designates free **cS**, the green band designates encapsulated **tS**, and the grey band designates protons of **C1** after **tS** encapsulation. All the spectra were recorded in D_2O at 298 K. DFT optimized structure of **cS@C1**: (e) side view, (f) top view. Colour codes of host: carbon (yellow), nitrogen (deep blue), oxygen (red), palladium (grey). Colour codes of guest: carbon (magenta). Hydrogen atoms are omitted for clarity.

transient C-C single bond of **tS** following UV-excitation (which is required for isomerizing to the cis isomer, **cS**). On the other hand, **cS** can be photo-switched back to **tS** using visible light irradiation. Interestingly, when the host–guest complex **cS@C1** in aqueous media was irradiated with a light source of 446 nm for 3 h, the ^1H NMR portrayed a different story (Figure S40). The ^1H NMR of the host–guest complex, **cS@C1**, after irradiation resembled **tS@C1** along with the unencapsulated **cS** peaks. However, no encapsulated **cS** peaks were present (Figure S40). A possible explanation for this observation is the weak absorption of **C1** at 446 nm (Figure S37), which doesn't interfere with the photoconversion of **cS** to **tS** within the cavity of **C1** and its preference for **tS**. The encapsulated **cS** and free **cS** are in a dynamic equilibrium that converts to less polar E-form (**tS**) upon 446 nm irradiation, which is rapidly "caged" out of solution

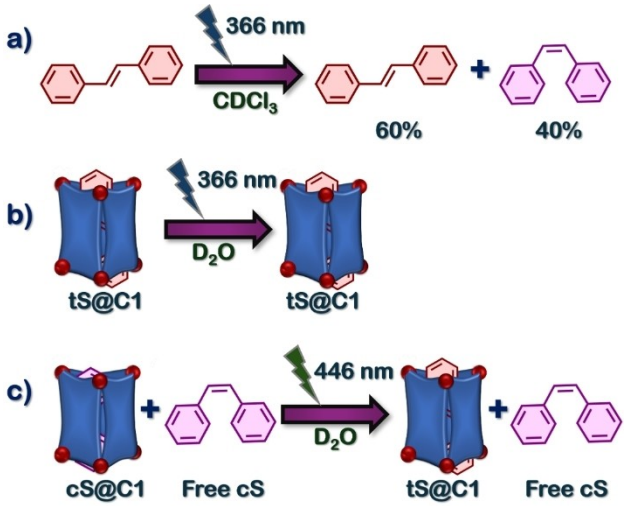

Scheme 5. Schematic representation of photo-isomerization: (a) **tS** upon irradiation with a light source of 366 nm for 8 h in $CDCl_3$, (b) no photo-isomerization of **tS@C1** upon irradiation with a light source of 366 nm for 8 h in D_2O, (c) photo-isomerization of **cS@C1** to **tS@C1** upon irradiation with a visible light source of 446 nm for 3 h in D_2O.

by the hydrophobic cavity of **C1**. However, the free excess **cS** in the aqueous reaction mixture (due to partial solubility of **cS** in water) remain as **cS** since the more polar **cS** form is stabilized by polar solvent water that resists easy photo-isomerization back to E-form, **tS** (Scheme 5c). Thus, **C1** facilitates the reverse isomerization of **cS** to **tS**.

Conclusion

We report here the synthesis of a Pd_6 trifacial tubular barrel (**C1**) via the coordination self-assembly of a 90° Pd(II) acceptor with a fluorenone-embedded coordinatively flexible tetra-pyridyl ligand (**L**). The higher co-ordinational flexibility of the ligand, in addition to the dynamic nature of Pd–N bonding, enabled **C1** to transform to a non-isomeric higher order Pd_{12} triangular orthobicupola (**C2**) architecture in the presence of various external stimuli. Crystallization induced the formation of **C2** along with **C1** from the aqueous solution of **C1**, which implied that increased concentration induced **C2** formation. Additionally, solvent and counter-anion played a crucial role in such structural conversion. The NO_3^- analogue in a 3:2 water-acetonitrile mixture exists as a mixture of **C1** and **C2** in an 89:11 ratio. On the other hand, the PF_6^- analogue in acetonitrile exists as majorly **C1** at room temperature which completely converts to **C2** irreversibly upon heat treatment. Thus, a temperature dependence was also observed for PF_6^- analogue in acetonitrile. In summary, the self-assembly of ligand (**L**) with a 90° Pd(II) acceptor (**M**) generated a stimuli-responsive system that effectively toggled between two energy-minimized architectures, which can be controlled by modulating the external signal (stimuli) applied to the system. Stimuli-induced generation of such an unusual triangular ortho-bicupola architecture (**C2**) from a completely different non-isomeric self-assembled product (trifacial barrel, **C1**) in solution is a unique phenomenon.

The inclination of the trifacial barrel (**C1**) to act as a selective host for *trans*-stilbene (**tS**) was explored. **C1** has a compatible cavity size to stabilize one molecule of **tS** within its cavity. This stabilization was facilitated by the multiple H-bonding interactions between the inwardly oriented fluorenone oxygen atoms of the host and guest C–H protons. Moreover, **C1** showcased its potential in selective recognition of **tS** from a 1:1 mixture of **tS** and **cS**. Furthermore, **C1,** by strongly stabilizing **tS** within its cavity, preventing the free rotation of encapsulated **tS** about transient C–C single bond of **tS** following UV-excitation, and by partly absorbing incoming UV irradiation was effective in intercepting the conversion of **tS** to **cS** within its cavity. Moreover, **C1** facilitated the reverse isomerization of encapsulated **cS** (**cS@C1**) to **tS@C1** under visible light irradiation in a polar aqueous media, which otherwise stabilizes the polar **cS** form and resists easy photo-switching to **tS** form.

In conclusion, we successfully synthesized a self-assembled system (**C1**) in aqueous solution that can selectively recognize **tS** from a mixture of **tS** and **cS**. **C1** was proved to act as a potent host that strongly stabilized **tS** and worked as a UV-guard that hindered the transformation of **tS** to **cS** but facilitated the reverse visible light-induced photoconversion of **cS** to **tS** within its cavity. Supplementarily, **C1** was able to migrate to a non-analogous architecture **C2** driven by different external signals, rendering it stimuli responsive.

Author Contributions

P.S.M., M.A. and R.B. devised the project and designed the experiments. M.A. mostly carried out all the experimental work. M.A. and R.B. analysed the results. N.H. carried out the crystallographic studies in Italy. R.B. carried out the optimization studies. All the authors were involved in writing the manuscript, and they have given approval to the final version of the manuscript.

Acknowledgements

P.S.M. thanks the SERB (New Delhi) for the research grant and for J. C. Bose Fellowship. M.A. gratefully acknowledges IISc for research fellowship. R.B. acknowledges PMRF (India) for research fellowship and contingency grant.

Conflict of Interest

The authors declare no conflict of interest.

Data Availability Statement

The data that support the findings of this study are available in the supplementary material of this article.

Keywords: Self-assembly · Coordination Cages · Structural transformation · Stimuli-responsive behavior · Host-Guest Chemistry

[1] M. Fujita, M. Tominaga, A. Hori, B. Therrien, *Acc. Chem. Res.* **2005**, *38*, 369–378.
[2] R. Saha, B. Mondal, P. S. Mukherjee, *Chem. Rev.* **2022**, *122*, 12244–12307.
[3] E. G. Percástegui, T. K. Ronson, J. R. Nitschke, *Chem. Rev.* **2020**, *120*, 13480–13544.
[4] S. R. Seidel, P. J. Stang, *Acc. Chem. Res.* **2002**, *35*, 972–983.
[5] K. Wu, E. Benchimol, A. Baksi, G. H. Clever, *Nat. Chem.* **2024**, *16*, 584–591.
[6] H. Liu, Z. Zhang, C. Mu, L. Ma, H. Yuan, S. Ling, H. Wang, X. Li, M. Zhang, *Angew. Chem. Int. Ed.* **2022**, *61*, e202207289.
[7] N. Kishida, Y. Tanaka, M. Yoshizawa, *Chem. Eur. J.* **2022**, *28*, e202202075.
[8] W.-X. Gao, H.-J. Feng, B.-B. Guo, Y. Lu, G.-X. Jin, *Chem. Rev.* **2020**, *120*, 6288–6325.
[9] R. Chakrabarty, P. S. Mukherjee, P. J. Stang, *Chem. Rev.* **2011**, *111*, 6810–6918.
[10] W. Liu, Y. Tan, L. O. Jones, B. Song, Q.-H. Guo, L. Zhang, Y. Qiu, Y. Feng, X.-Y. Chen, G. C. Schatz, J. F. Stoddart, *J. Am. Chem. Soc.* **2021**, *143*, 15688–15700.
[11] S. Freye, J. Hey, A. Torras-Galán, D. Stalke, R. Herbst-Irmer, M. John, G. H. Clever, *Angew. Chem. Int. Ed.* **2012**, *51*, 2191–2194.
[12] C. Jiang, S.-J. Hu, L.-P. Zhou, J. Yang, Q.-F. Sun, *Chem. Commun.* **2022**, *58*, 5494–5497.
[13] A. E. Martín Díaz, J. E. M. Lewis, *Front. Chem.* **2021**, *9*, 70642.
[14] T. Tateishi, M. Yoshimura, S. Tokuda, F. Matsuda, D. Fujita, S. Furukawa, *Coord. Chem. Rev.* **2022**, *467*, 214612.
[15] L.-L. Yan, L.-Y. Yao, M. Ng, V. W.-W. Yam, *J. Am. Chem. Soc.* **2021**, *143*, 19008–19017.
[16] L.-X. Cai, D.-N. Yan, P.-M. Cheng, J.-J. Xuan, S.-C. Li, L.-P. Zhou, C.-B. Tian, Q.-F. Sun, *J. Am. Chem. Soc.* **2021**, *143*, 2016–2024.
[17] T.-Z. Xie, K. J. Endres, Z. Guo, J. M. Ludlow, III, C. N. Moorefield, M. J. Saunders, C. Wesdemiotis, G. R. Newkome, *J. Am. Chem. Soc.* **2016**, *138*, 12344–12347.
[18] Y. Lu, Y.-X. Deng, Y.-J. Lin, Y.-F. Han, L.-H. Weng, Z.-H. Li, G.-X. Jin, *Chem* **2017**, *3*, 110–121.
[19] B. Kilbas, S. Mirtschin, R. Scopelliti, K. Severin, *Chem. Sci.* **2012**, *3*, 701–704.
[20] J. Ramírez, A.-M. Stadler, N. Kyritsakas, J.-M. Lehn, *Chem. Commun.* **2007**, 237–239.
[21] H. Lee, J. Han, D. Kim, O.-S. Jung, *Dalton Trans.* **2021**, *50*, 14849–14854.
[22] H.-J. Yu, Z.-M. Liu, M. Pan, K. Wu, Z.-W. Wei, Y.-W. Xu, Y.-N. Fan, H.-P. Wang, C.-Y. Su, *Eur. J. Inorg. Chem.* **2018**, *2018*, 80–85.
[23] W. M. Bloch, J. J. Holstein, B. Dittrich, W. Hiller, G. H. Clever, *Angew. Chem. Int. Ed.* **2018**, *57*, 5534–5538.
[24] S. Wang, T. Sawada, K. Ohara, K. Yamaguchi, M. Fujita, *Angew. Chem. Int. Ed.* **2016**, *55*, 2063–2066.
[25] D. M. Wood, W. Meng, T. K. Ronson, A. R. Stefankiewicz, J. K. M. Sanders, J. R. Nitschke, *Angew. Chem. Int. Ed.* **2015**, *54*, 3988–3992.
[26] R. Banerjee, D. Chakraborty, W.-T. Jhang, Y.-T. Chan, P. S. Mukherjee, *Angew. Chem. Int. Ed.* **2023**, *62*, e202305338.
[27] R. Banerjee, S. Bhattacharyya, P. S. Mukherjee, *JACS Au* **2023**, *3*, 1998–2006.
[28] R. Banerjee, D. Chakraborty, P. S. Mukherjee, *J. Am. Chem. Soc.* **2023**, *145*, 7692–7711.
[29] M. Zhang, M. L. Saha, M. Wang, Z. Zhou, B. Song, C. Lu, X. Yan, X. Li, F. Huang, S. Yin, P. J. Stang, *J. Am. Chem. Soc.* **2017**, *139*, 5067–5074.
[30] S. Maji, J. Samanta, R. Natarajan, *Chem. Eur. J.* **2024**, *30*, e202303596.
[31] A. Chowdhury, P. Howlader, P. S. Mukherjee, *Chem. Eur. J.* **2016**, *22*, 7468–7478.
[32] P. C. Purba, M. Venkateswaralu, S. Bhattacharyya, P. S. Mukherjee, *Inorg. Chem.* **2022**, *61*, 713–722.
[33] A. B. Sainaba, R. Saha, M. Venkateswarulu, E. Zangrando, P. S. Mukherjee, *Inorg. Chem.* **2024**, *63*, 508–517.
[34] E. O. Bobylev, J. Ruijter, D. A. Poole Iii, S. Mathew, B. de Bruin, J. N. H. Reek, *Angew. Chem. Int. Ed.* **2023**, *62*, e202218162.
[35] V. Martí-Centelles, A. L. Lawrence, P. J. Lusby, *J. Am. Chem. Soc.* **2018**, *140*, 2862–2868.
[36] S. M. Bierschenk, R. G. Bergman, K. N. Raymond, F. D. Toste, *J. Am. Chem. Soc.* **2020**, *142*, 733–737.
[37] L. R. Holloway, P. M. Bogie, Y. Lyon, C. Ngai, T. F. Miller, R. R. Julian, R. J. Hooley, *J. Am. Chem. Soc.* **2018**, *140*, 8078–8081.
[38] Y. Nishioka, T. Yamaguchi, M. Yoshizawa, M. Fujita, *J. Am. Chem. Soc.* **2007**, *129*, 7000–7001.
[39] D. Chakraborty, S. Ali, P. Choudhury, N. Hickey, P. S. Mukherjee, *J. Am. Chem. Soc.* **2023**, *145*, 26973–26982.
[40] P. Das, A. Kumar, P. Howlader, P. S. Mukherjee, *Chem. Eur. J.* **2017**, *23*, 12565–12574.
[41] D. Samanta, P. S. Mukherjee, *Chem. Commun.* **2013**, *49*, 4307–4309.
[42] C. J. Hastings, M. D. Pluth, R. G. Bergman, K. N. Raymond, *J. Am. Chem. Soc.* **2010**, *132*, 6938–6940.
[43] W.-Y. Zhang, Y.-J. Lin, Y.-F. Han, G.-X. Jin, *J. Am. Chem. Soc.* **2016**, *138*, 10700–10707.
[44] G. Li, W. Yu, J. Ni, T. Liu, Y. Liu, E. Sheng, Y. Cui, *Angew. Chem. Int. Ed.* **2008**, *47*, 1245–1249.
[45] D. Zhang, T. K. Ronson, R. Lavendomme, J. R. Nitschke, *J. Am. Chem. Soc.* **2019**, *141*, 18949–18953.
[46] L. Catti, R. Sumida, M. Yoshizawa, *Coord. Chem. Rev.* **2022**, *460*, 214460.
[47] A. B. Sainaba, M. Venkateswarulu, P. Bhandari, K. S. A. Arachchige, J. K. Clegg, P. S. Mukherjee, *J. Am. Chem. Soc.* **2022**, *144*, 7504–7513.
[48] D. Chakraborty, R. Saha, J. K. Clegg, P. S. Mukherjee, *Chem. Sci.* **2022**, *13*, 11764–11771.
[49] A. B. Grommet, L. M. Lee, R. Klajn, *Acc. Chem. Res.* **2020**, *53*, 2600–2610.
[50] P. Mal, B. Breiner, K. Rissanen, J. R. Nitschke, *Science* **2009**, *324*, 1697–1699.
[51] P. Howlader, B. Mondal, P. C. Purba, E. Zangrando, P. S. Mukherjee, *J. Am. Chem. Soc.* **2018**, *140*, 7952–7960.
[52] R. Saha, A. Devaraj, S. Bhattacharyya, S. Das, E. Zangrando, P. S. Mukherjee, *J. Am. Chem. Soc.* **2019**, *141*, 8638–8645.
[53] R. A. Tromans, T. S. Carter, L. Chabanne, M. P. Crump, H. Li, J. V. Matlock, M. G. Orchard, A. P. Davis, *Nat. Chem.* **2019**, *11*, 52–56.
[54] V. Abdul Rinshad, J. Sahoo, M. Venkateswarulu, N. Hickey, M. De, P. Sarathi Mukherjee, *Angew. Chem. Int. Ed.* **2023**, *62*, e202218226.
[55] G. Gupta, Y. Sun, A. Das, P. J. Stang, C. Yeon Lee, *Coord. Chem. Rev.* **2022**, *452*, 214308.
[56] Z. Zhang, Z. Zhao, Y. Hou, H. Wang, X. Li, G. He, M. Zhang, *Angew. Chem. Int. Ed.* **2019**, *58*, 8862–8866.
[57] P.-P. Jia, L. Xu, Y.-X. Hu, W.-J. Li, X.-Q. Wang, Q.-H. Ling, X. Shi, G.-Q. Yin, X. Li, H. Sun, Y. Jiang, H.-B. Yang, *J. Am. Chem. Soc.* **2021**, *143*, 399–408.
[58] A. Kumar, R. Saha, P. S. Mukherjee, *Chem. Sci.* **2021**, *12*, 5319–5329.

[59] K. Acharyya, S. Bhattacharyya, H. Sepehrpour, S. Chakraborty, S. Lu, B. Shi, X. Li, P. S. Mukherjee, P. J. Stang, *J. Am. Chem. Soc.* **2019**, *141*, 14565–14569.
[60] W. Xue, L. Pesce, A. Bellamkonda, T. K. Ronson, K. Wu, D. Zhang, N. Vanthuyne, T. Brotin, A. Martinez, G. M. Pavan, J. R. Nitschke, *J. Am. Chem. Soc.* **2023**, *145*, 5570–5577.
[61] P. Howlader, P. Bhandari, D. Chakraborty, J. K. Clegg, P. S. Mukherjee, *Inorg. Chem.* **2020**, *59*, 15454–15459.
[62] S. Dey, M. Aggarwal, D. Chakraborty, P. S. Mukherjee, *Chem. Commun.* **2024**, *60*, 5573–5585.
[63] I. A. Bhat, R. Jain, M. M. Siddiqui, D. K. Saini, P. S. Mukherjee, *Inorg. Chem.* **2017**, *56*, 5352–5360.
[64] D. Villarón, S. J. Wezenberg, *Angew. Chem. Int. Ed.* **2020**, *59*, 13192–13202.
[65] T. J. Bannin, P. P. Datta, E. T. Kiesewetter, M. K. Kiesewetter, *J. Chem. Educ.* **2019**, *96*, 143–147.
[66] S. Bhattacharyya, M. Venkateswarulu, J. Sahoo, E. Zangrando, M. De, P. S. Mukherjee, *Inorg. Chem.* **2020**, *59*, 12690–12699.
[67] Deposition numbers CCDC 2352229 (for **C1**), CCDC 2352228 (for **C2**), contain the supplementary crystallographic data for this paper. These data are provided free of charge by the joint Cambridge Crystallographic Data Centre and Fachinformationszentrum Karlsruhe Access Structures service.